Apparent bipolarity and Seebeck sign inversion in a layered semiconductor: LaZnOP

Kentaro Kayanuma, Hidenori Hiramatsu, and Masahiro Hirano*
ERATO-SORST, Japan Science and Technology Agency (JST), in the Frontier Research Center, S2-6F East, Mail-box S2-13, Tokyo Institute of Technology, 4259 Nagatsuta-cho, Midori-ku, Yokohama 226-8503, Japan

Ryuto Kawamura, Hiroshi Yanagi, and Toshio Kamiya†
Materials and Structures Laboratory, Mail-box R3-1, Tokyo Institute of Technology, 4259 Nagatsuta-cho, Midori-ku, Yokohama 226-8503, Japan

Hideo Hosono†,‡
Frontier Research Center, S2-6F East, Mail-box S2-13, Tokyo Institute of Technology, 4259 Nagatsuta-cho, Midori-ku, Yokohama 226-8503, Japan
(Received 27 August 2007; published 26 November 2007)

The optoelectronic properties of a layered mixed-anion compound, LaZnOP, which is expected to be a wide gap *n*-type semiconductor, are examined. LaZnOP shows electronic conduction with conductivities up to 5.2 S/cm at room temperature by Cu doping. The signs of Seebeck coefficients suggest that undoped LaZnOP is typically an *n*-type semiconductor, but Cu-doped LaZnOP is a *p*-type. However, the Seebeck coefficients are very small compared to those observed for isostructural *p*-type semiconductors, LaCuO*Ch* (*Ch*=S,Se), and show a sign inversion as the temperature is varied in the undoped and Zr-doped LaZnOP. The optical band gap is 1.3–1.7 eV, which is much smaller than those of related compounds such as LaCuOS (3.1 eV) and ZnO (3.3 eV). These properties can be understood by the electronic structure obtained using photoemission spectroscopy (PES) and *ab initio* band calculations. The results indicate that the synthesized LaZnOP has subgap states that pin the Fermi level, and these subgap states form a defect band, which gives the abnormally small Seebeck coefficients and their inversion with temperature. The band calculations suggest that anion defects may be the origin of the defect band implied by the PES measurements and control the observed electrical characteristics.

DOI: 10.1103/PhysRevB.76.195325 PACS number(s): 72.20.−i, 71.55.−i, 79.60.Bm, 71.15.Mb

I. INTRODUCTION

Wide gap semiconductors have attracted much attention because they are strong candidate materials for light-emitting diodes (LEDs) operating in the blue-to-ultraviolet region.[1] To be applicable to short-wavelength LEDs, materials must have (i) a large band gap compatible with that of the light-emitting layer, (ii) a small hole injection barrier with the hole transport or light-emitting layer, and (iii) a high electronic conductivity to reduce series resistance. However, such a material currently does not exist because high-density hole doping becomes more difficult as the band gap becomes larger. We have reported the optical and electrical properties of layered oxychalcogenides, LaCuO*Ch* (*Ch*=chalcogen ions),[2] and found that LaCuO*Ch* has properties superior to those of other wide gap *p*-type semiconductors such as GaN:Mg,[3,4] ZnSe:N,[5] and ZnO:N.[6] For example, Mg-doped LaCuOSe (band gap ~2.8 eV) exhibits degenerate *p*-type conduction,[7,8] which has yet to be attained for other wide gap *p*-type semiconductors. Furthermore, LaCuO*Ch* shows a sharp photoluminescence in the blue-to-ultraviolet region, which originates from room-temperature stable excitons.[9–11] These superior properties may be attributed to the layered crystal structure composed of LaO and Cu*Ch* layers,[12–16] where the Cu*Ch* layers form hole transport paths[17] (the crystal structure is shown in Fig. 1). Utilizing these features, we have demonstrated room-temperature operation of an excitonic blue LED.[18] The LED employed a hetero-*p*/*n*-junction structure, which was composed of a light-emitting *p*-type LaCuOSe epilayer and an electron-injection amorphous *n*-type In-Ga-Zn-O layer. Although a homostructural junction should exhibit better device performance, an *n*-type material from an isostructural compound of LaCuOSe has yet to be found. Therefore, we have surveyed *n*-type semiconductors with similar crystal structures, which include $La_2CdO_2Se_2$ (Ref. 19) and $La_2SnO_2S_3$.[20] However, all surveyed semiconductors were *p*-type semiconductors or very resistive. Thus, we extended the survey to layered oxypnictides, La*MOPn* (*M*=divalent cations, *Pn*=pnicogen ions), with the same crystal structure as LaCuO*Ch* (Fig. 1).[21–25] Among them, we noticed that LaZnO*Pn* is a candidate for an *n*-type semiconductor because Zn-based oxides such as ZnO and $InGaZnO_4$ (Ref. 26) are well-known wide gap *n*-type conductors.

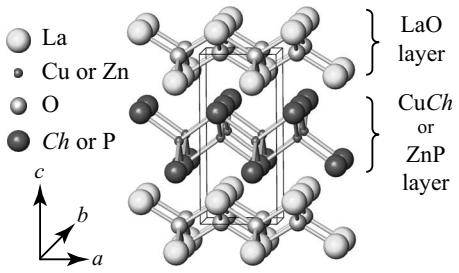

FIG. 1. Crystal structure of LaCuO*Ch* (*Ch*=chalcogen ions) and LaZnOP, which have layered crystal structures composed of LaO and Cu*Ch*/ZnP layers.

In this work, we examined the optoelectronic properties and the effects of impurity doping of LaZnOP along with the electronic structures. Thermopower measurements appear to indicate that bipolar doping is achieved in LaZnOP because the Seebeck coefficients of nominally undoped LaZnOP are typically negative, but those of Cu-doped LaZnOP are positive. However, unconventional results are also observed in the thermopower measurements; their values are too small to be understood as band conductors and show a sign inversion when varying the temperature. Ultraviolet photoemission spectroscopy (UPS) measurements show that the Fermi level is not altered by Cu doping, suggesting that the synthesized LaZnOP has pinning states in the band gap, and the observed electrical conductivities are attributed to the subgap band. These results are a reminder that standard characterization procedures such as Hall measurements and thermopower measurements to determine carrier polarity do not always work properly. Thus, careful assessments are required to reach a final conclusion, especially for heavily doped materials. The origin of the difficulty in *n*-type doping in this Zn-based compound is discussed on the basis of the band alignment built from UPS measurements.

II. EXPERIMENT AND CALCULATION

Growth of LaZnOP single crystals has been reported by Nientiedt and Jeitschko using a flux method,[23] but they did not report the optoelectronic properties. Recently, Takano *et al.* have reported the electrical and magnetic properties of *Ln*ZnO*Pn* (*Ln*=lanthanides, *Pn*=pnicogens) sintered ceramics samples.[27] Their LaZnOP sample, which was synthesized from La_2O_3, La, Zn, and P, has an insulating nature. Employing a similar synthesis using La_2O_3, Zn_3P_2, La, and P as starting materials, we reproduced this result and obtained only insulating samples.[28] Therefore, we chose a different synthetic route to obtain conductive samples. First, the starting material, LaP, was prepared by heating a stoichiometric mixture of La and P at 700 °C for 10 h in an evacuated silica glass tube. Then, a stoichiometric mixture of the synthesized LaP and reagent ZnO powder was pressed into pellets. Finally, the pressed pellet was sealed in an evacuated silica glass tube and subsequently heated at 1000 °C for 10 h. Because the powders, especially La, P, and LaP, are reactive in an air and a moist atmosphere, all the mixing and pressing procedures were carried out in a glovebox (made by Miwa Mfg.) filled with a dry Ar gas at a dew point of about −70 °C. High-density ceramics samples were prepared by a spark plasma sintering (SPS-515S made by SPS SYNTEX) technique for dc electrical conductivity and photoemission measurements (apparent densities >90%). To increase the carrier density and alter the carrier polarity, impurity doping was examined using Cu, Zr, Hf, Sr, and Ca as dopants. To synthesize the doped samples, LaP, ZnO, La_2O_3, Zn_3P_2, Cu_3P, ZrO_2, HfO_2, SrO, CaO, Zn, and P were mixed at compositions of $(La_{0.9}M_{0.1})$ZnOP (*M*=Cu, Zr, Hf, Sr, and Ca) using the above synthetic process.

The purity and crystal structure of the obtained samples were characterized by powder x-ray diffraction (XRD) (D8 ADVANCE-TXS made by Bruker AXS) using Cu $K\alpha$ radiation (power: 45 kV×360 mA) and a solid-state detector (called as Sol-X). Lattice parameters and crystal structure were refined by the Rietveld method using the code TOPAS3 based on the fundamental parameter approach for the Bragg-Brentano geometry.[29]

dc electrical conductivities of sintered polycrystalline samples with sputtered Pt electrodes were measured by a four-probe method in the temperature range from 50 up to 400 K using a physical property measurement system (made by Quantum Design). Thermopower measurements were performed from 300 to 50 K to obtain Seebeck coefficients and to determine carrier polarity. To estimate optical band gaps, diffuse reflectance spectra (R_{obs}) of the undoped LaZnOP were measured with powder samples diluted with a small amount of KBr powder and converted to absorption spectra using the Kubelka-Munk equation, $(1-R_{obs})^2/(2R_{obs})=\alpha/s$, where α and s denote an absorption coefficient and a scattering factor, respectively.[30]

Ultraviolet photoemission spectroscopy (UPS) measurements were conducted at room temperature using the He I emission lines (21.2 eV) with a hemispherical analyzer (Class 150 made by VSW). Inverse photoemission spectroscopy (IPES) measurements were conducted with a homemade instrument in a bremsstrahlung isochromat spectroscopy mode by detecting 9.5 eV photons emitted from the samples. To clean the surface for the UPS and IPES measurements, the sample surfaces were scraped with a diamond file in a vacuum of 3×10^{-9} Torr in a preparation chamber connected to the measurement chambers. The UPS and IPES measurements were performed at pressures of $<5\times10^{-9}$ and $<8\times10^{-10}$ Torr, respectively. Polycrystalline gold was used as a reference to calibrate the Fermi level of the samples. Work functions were estimated from the secondary electron cutoff energy in the UPS spectra using He I emission.

Density functional theory (DFT) periodic calculations were performed with the code VASP (Ref. 31) using a projector augmented plane wave method and PBE96 generalized gradient approximation functionals for stoichiometric and defect-containing LaZnOP. The initial model for the stoichiometric LaZnOP was the fundamental unit cell of LaZnOP, which contained a chemical formula unit of $(LaZnOP)_2$ with the experimental lattice parameters [$a=b=0.4040$ nm and $c=0.8908$ nm (Ref. 23)]. Those of defect-containing LaZnOP (i.e., $La_{18}Zn_{18}O_{18}P_{17}$, $La_{18}Zn_{18}O_{17}P_{18}$, $La_{18}Zn_{17}O_{18}P_{18}$, and $La_{17}Zn_{18}O_{18}P_{18}$) were based on $3\times3\times1$ superlattice cells containing the $(LaZnOP)_{18}$ unit. To obtain quantum-mechanically stable structures, DFT calculations were used to relax the lattice parameters and atomic positions. Band structures and projected density of states were calculated based on the relaxed structures. For all the calculations, the cutoff energy for the basis sets was set to 200 eV.

III. RESULTS AND DISCUSSION

Figure 2 shows the observed XRD pattern of undoped LaZnOP. The simulated pattern by the Rietveld method agrees well with the measured XRD pattern, as shown in the difference profile, and extra peaks are not observed, indicating a single-phase sample was obtained. The crystal structure

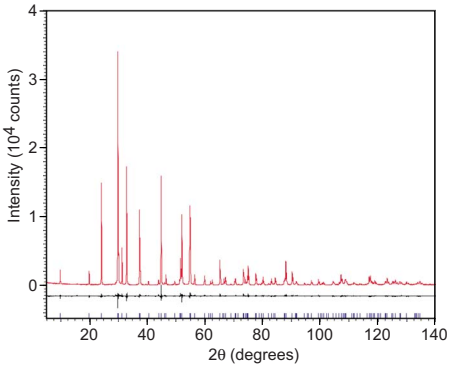

FIG. 2. (Color online) XRD pattern of undoped LaZnOP powder and the result of Rietveld analysis. (Upper row) observed pattern. (Middle row) Difference profile between the observed and simulated patterns. (Bottom row) Positions of Bragg reflections.

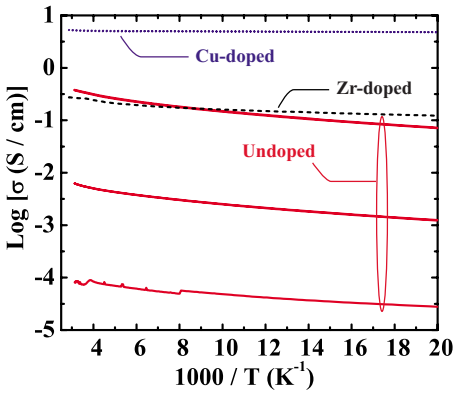

FIG. 3. (Color online) Electrical conductivities of undoped, Cu-doped, and Zr-doped LaZnOP as a function of temperature.

refined by the Rietveld analysis (Table I) agrees well with the previous report on the single crystal.[23] The single-phase powder was light brown.

Figure 3 shows the temperature dependence of electrical conductivities of the undoped, 10 at. % Zr-doped, and 10 at. % Cu-doped LaZnOP. The electrical conductivity at room temperature (RT) of the undoped LaZnOP ranged from 7.6×10^{-5} to 3.6×10^{-1} S/cm due to the deviation of the sample preparation batches but decreased slightly as the temperature decreased, regardless of the RT conductivity. These features, the high conductivity and nearly degenerate conduction, suggest that although all the previously reported samples were insulators,[27,28] somewhat high-density carriers are introduced to the nominally undoped LaZnOP. These carriers are probably due to the nonstoichiometry of our samples. The estimated apparent activation energy was ~11 meV around RT. It should be noted that this result (i.e., the apparent activation energy did not change, but the RT conductivity varied more than 3 orders of magnitude) is not usual for orthodox crystalline semiconductors, as will be discussed later. It is confirmed that 10 at. % doping of Zr, Hf, Sr, and Ca does not increase the conductivity higher than that of the most conductive undoped sample. However, Cu doping enhanced the electrical conductivity to 5.2 S/cm, and the temperature dependence of conductivity nearly vanished.

Next, Seebeck coefficients were evaluated from the thermopower measurements. The results gave a negative value of −2.7 μV/K for the sample with the highest conductivity (3.6×10^{-1} S/cm for undoped LaZnOP at room temperature, indicated by the open squares in Fig. 4), but a positive value of +12 μV/K was obtained for the Cu-doped LaZnOP (the closed symbol). These observations suggest that undoped LaZnOP is an *n*-type semiconductor, but Cu-doped LaZnOP is a *p*-type one. However, these values are very small, e.g., compared to those obtained for LaCuO*Ch* epitaxial films.[7] In addition, the Seebeck coefficients of the other undoped LaZnOP samples with different electrical conductivities (i.e., different carrier concentrations) do not show systematic variations with conductivity (Fig. 4). It is known that the Seebeck coefficient decreases as the carrier concentration (n_c) increases with the dependence of log n_c for a nondegenerated band semiconductors. Considering the relation $\sigma = en_c\mu$ (σ is electronic conductivity, e the elementary electric charge, and μ the drift mobility), the Seebeck coefficient roughly depends on the logarithm of electronic conductivity based on the supposition of a constant mobility. Therefore, the results that the Seebeck coefficient of LaZnOP does not change with the electrical conductivity and is smaller by 1 or 2 orders of magnitude compared to those of isostructural

TABLE I. Crystal structures of LaZnOP refined by the present Rietveld analysis, determined by the single-crystal structure analysis in Ref. 23, and obtained by structure relaxation calculation by DFT.

	a (nm)	*c* (nm)	R_p (%)	R_{wp} (%)	R_{ex} (%)	Goodness of fit
This work	0.404109(1)	0.890486(3)	5.74	8.01	5.01	1.60
Ref. 23	0.4040(1)	0.8908(2)				
DFT	0.4046	0.8942				
	x	*y*	*Z* (this work)	*z* (Ref. 23)		*z* (DFT)
La	1/4	1/4	0.13902(4)	0.13870(5)		0.1390
Zn	3/4	1/4	1/2			
O	3/4	1/4	0			
P	1/4	1/4	0.6638(2)	0.6646(2)		0.6641

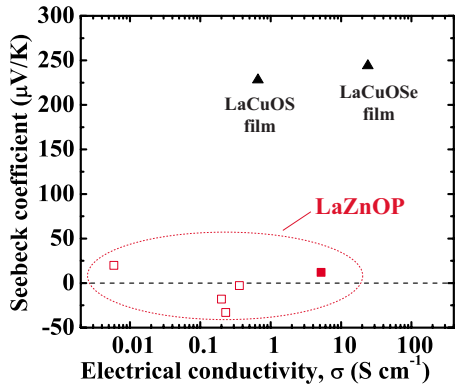

FIG. 4. (Color online) Seebeck coefficients of undoped (open squares) and Cu-doped (closed square) LaZnOP plotted against electrical conductivity at room temperature. Data of epitaxial films of undoped LaCuO*Ch* (Ref. 7) are shown by closed triangles for comparison.

semiconductors, LaCuO*Ch* (*Ch*=S,Se), are unreasonable (note that these values were obtained on epitaxial films, but the film microstructure is not essential to this discussion). In addition, a lower conductive (5.9×10^{-3} S/cm), undoped sample showed a positive Seebeck sign (Fig. 4), and the temperature dependences of the Seebeck coefficients showed that the sign of the Seebeck coefficients flipped for the undoped and Zr-doped LaZnOP (Fig. 5). These results suggest that the electrical conduction in LaZnOP polycrystalline samples is not a band conduction of electron and/or hole carriers.

Figure 6 shows the UPS spectra of the undoped (*n*-type) and Cu-doped (*p*-type) LaZnOP. Here, the binding energy was measured from the Fermi level of the samples. The intensity of the IPES spectrum was normalized so that it was comparable to those of the UPS spectra. Three bands A, B, and C were observed around ~10.5, 5.5, and 2.5 eV, respectively. From a DFT calculation as shown in Fig. 8(d), bands A will be assigned to Zn 3*d*–P 3*p* bonding states, and C to bonding states between Zn 3*d*–P 3*p* antibonding states and Zn 4*s*, respectively. The deep region of band B around 7 eV

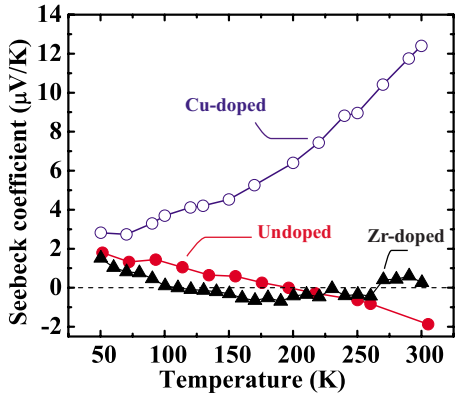

FIG. 5. (Color online) Temperature dependence of Seebeck coefficients of undoped (closed circles), Cu-doped (open circles), and Zr-doped (closed triangles) LaZnOP.

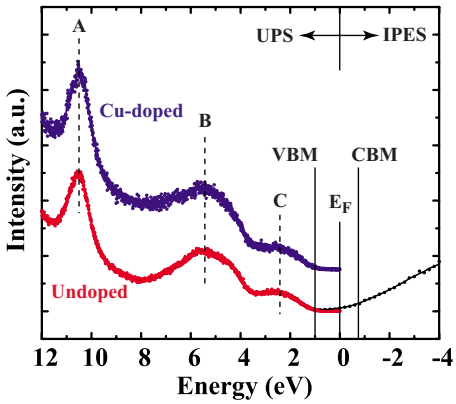

FIG. 6. (Color online) UPS (excitation photon energy =21.2 eV) spectra of undoped and Cu^+-doped LaZnOP. IPES spectrum is also shown for the undoped LaZnOP. E_F denotes the Fermi level.

is composed of Zn 4*s*–P 3*p* bonding states with smaller contribution of Zn 3*d*. The shallower region of band B is composed of O 2*p* slightly hybridized with La 5*s*, which are further split to bonding, nonbonding, and antibonding states of O-O bonds in the order from a deep energy to a shallower energy. The valence band maximum (VBM) onset energy was estimated to be ~1.0 eV below the Fermi level. It should be noted that the binding energies of the VBM, A, B, and C bands did not shift between these samples (i.e., the Fermi levels were the same with respect to an absolute energy origin, e.g., the vacuum level), but the electrical conductivity was nearly 2 orders of magnitude different and the RT Seebeck coefficients had opposite signs. These observations imply that the Fermi level is pinned, suggesting that an additional band exists in the fundamental band gap of LaZnOP at ~1.0 eV above the VBM. The subgap band model also explains why almost degenerated conduction was observed for all the samples, regardless of the wide range of conductivities (Fig. 3), by assuming that the number of electrons in the subgap bands differs and the Fermi level is in the subgap band.

The electronic structure was also examined from optical measurements. The optical absorption spectra were obtained from diffuse reflectance spectra to evaluate the band gap (Fig. 7). Three types of plots [a $(\alpha h\nu/s)^2$-$h\nu$ plot for the allowed direct transition model (s denotes a scattering factor), a $(\alpha/s)^{1/2}$-$h\nu$ plot for the indirect transition model, and a $(\alpha/\mathrm{sh}\nu)^{2/3}$-$h\nu$ for the forbidden direct transition model] were examined. Two band edge structures were observed around 1.3 and 1.7 eV both in the $(\alpha h\nu/s)^2$-$h\nu$ and $(\alpha/\mathrm{sh}\nu)^{2/3}$-$h\nu$ plots. The combined plot of the UPS spectrum and the IPES spectrum in Fig. 6 gives a band gap energy of 1.4±0.4 eV, which is consistent with both absorption edge energies.

Figure 8(a) shows the band structure of LaZnOP calculated by DFT along the high-symmetry k lines. Those of LaCuOS and ZnO are shown for comparison. The energy of these band structures were aligned using the calculated energy levels of O 2*s* and those measured from the Fermi level calculated for LaZnOP. The calculated band gap of LaZnOP

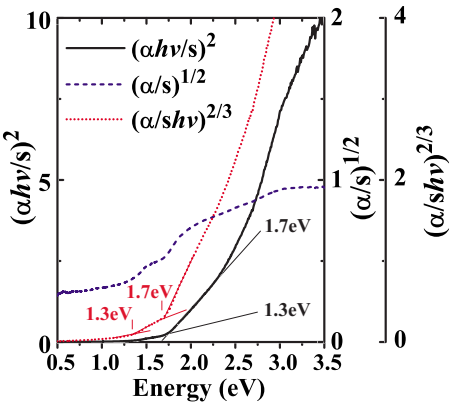

FIG. 7. (Color online) Absorption spectra of undoped LaZnOP converted from diffuse reflectance spectra using the Kubelka-Munk relation. Direct band gap is estimated from the $(\alpha h\nu/s)^2$-$h\nu$ plot (solid line), indirect band gap from the $(\alpha/s)^{1/2}$-$h\nu$ plot (dashed line), and direct forbidden band gap from the $(\alpha/sh\nu)^{2/3}$-$h\nu$ plot (dotted line).

was 0.75 eV, and both the VBM and conduction band minimum (CBM) were at the Γ point (k=0), indicating that LaZnOP is a direct-transition-type semiconductor. It should be noted that the calculated band gap values suffered from the well-known band gap problem of DFT, and they must be significantly underestimated. However, herein we simply compare this band structure to that of LaCuOS to qualitatively discuss the band gap of LaZnOP. LaCuOS was also determined to be a direct-transition-type semiconductor with an experimental optical gap of 3.1 eV,[9,17] but the band gap value obtained by DFT was 1.75 eV (b), which is smaller by 1.35 eV (the scissors operator) than the experimental value. Comparing these values, it appears reasonable that the band

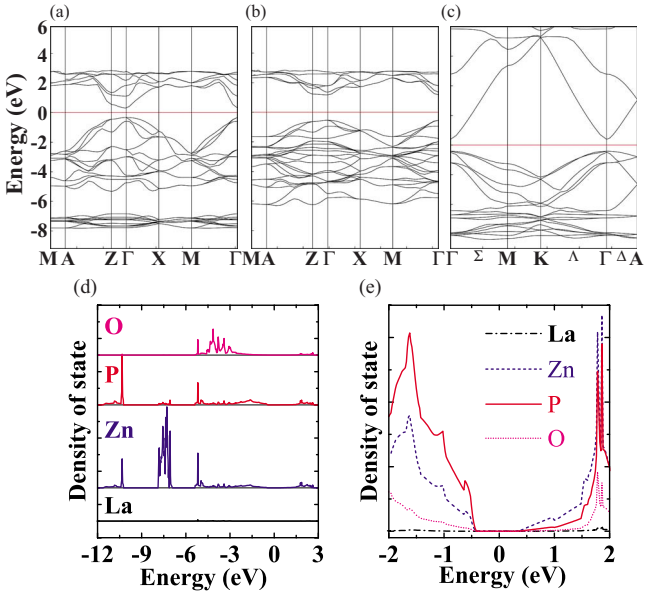

FIG. 8. (Color online) Band structures of (a) LaZnOP, (b) LaCuOS, and (c) ZnO. Energy is measured from the Fermi level of intrinsic LaZnOP. Horizontal lines show the Fermi levels. The energies are aligned using the O 2s levels. (d) Projected density of states. (e) Expanded view of (d) in the vicinity of the band gap.

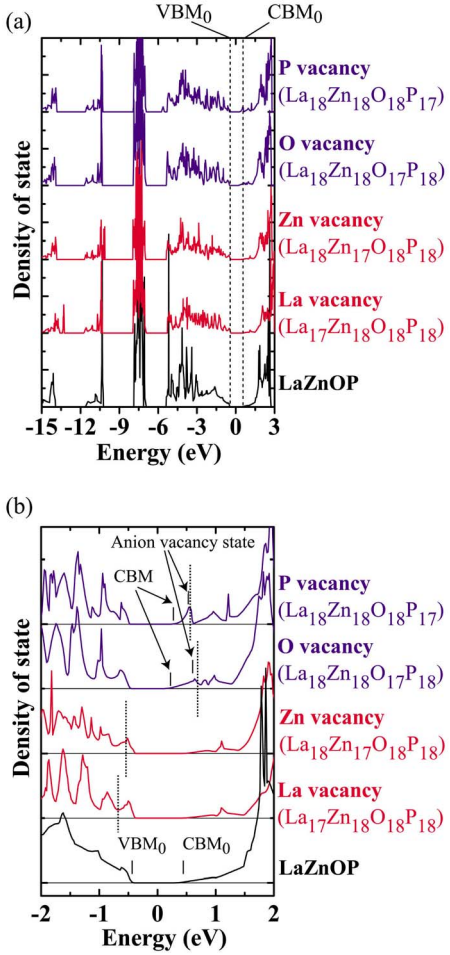

FIG. 9. (Color online) (a) Densities of states of defect-containing LaZnOP. That of stoichiometric LaZnOP is shown for comparison at the bottom. Energies are aligned with respect to the positions of P 3s around 10 eV. (b) Expanded view of (a). Vertical dashed lines indicate the Fermi levels, which separate the occupied states and unoccupied states.

gap of LaZnOP is smaller than that of LaCuOS and its scissors operator may also be around 1 eV. In addition, the calculated result indicates that the dipole transition between the VBM and CBM is allowed. These results, along with the above absorption spectrum analyses, indicate that LaZnOP is an allowed direct-transition-type semiconductor with a band gap of 1.3–1.7 eV (this point will be discussed again later).

The density of states [Figs. 8(d) and 8(e)] shows that the VBM of LaZnOP is mainly composed of P 3p orbitals and the CBM of Zn 4s. Comparing this result to Fig. 6, peaks A, B, and C in the UPS spectrum are attributed to mainly the Zn 3d, O 2p, and P 3p levels, respectively (detailed assignments were described above), although the absolute values of the calculated peak positions are smaller because the one-electron eigenvalue of DFT corresponds to a chemical potential and is smaller than the corresponding ionization energy.

As for the Fermi level pinning and the subgap states, which are speculated from the Seebeck anomaly and the UPS results, a possible explanation is that nonstoichiometric defects are formed in the synthesized samples, which form a

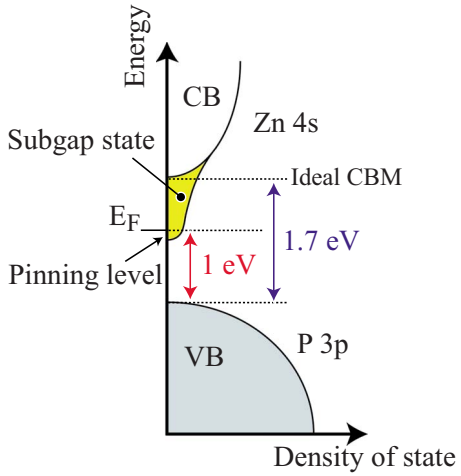

FIG. 10. (Color online) Schematic illustration of the electronic structure of anion-deficient LaZnOP.

conducting defect band. Thus, we calculated the electronic structures of defect-containing LaZnOP based on a supercell containing a $La_{18}Zn_{18}O_{18}P_{18}$ chemical unit. That is, $La_{18}Zn_{18}O_{18}P_{17}$ has a P vacancy, $La_{18}Zn_{18}O_{17}P_{18}$ has an O vacancy, and so on. Figure 9 shows that the cation vacancies form additional states in the vicinity of the VBM of the stoichiometric LaZnOP (VBM_0), and the Fermi levels are located below the VBM_0 by keeping the VBM level similar to the VBM_0. These results suggest that cationic vacancies introduce holes. In contrast, anion vacancies form additional states in the vicinity of the CBM of the stoichiometric LaZnOP (CBM_0), which reduce the CBM energies so that they are lower than the CBM_0: i.e., the CBM_0 is 0.75 eV above the VBM_0 for the stoichiometric LaZnOP, but the CBM of $La_{18}Zn_{18}O_{18}P_{17}$ is 0.70 eV and that of $La_{18}Zn_{18}O_{17}P_{18}$ is 0.63 eV. The density of states in the anion vacancy-containing LaZnOP shows sharp peak structures in the vicinity of the CBM and around the Fermi level, especially for the P vacancy case. The calculated band structure also confirms that the energy band at the Fermi level in the P vacancy-containing LaZnOP is narrow, ~0.3 eV in width. Similar results were obtained also for the O vacancy case. These results indicate that the anion vacancy states are localized. These localized states near the CBM_0 would be a plausible explanation for the subgap states observed by the UPS spectra. If this model is correct, then the higher absorption edge in Fig. 7 would correspond to the fundamental band gap of stoichiometric LaZnOP, while the lower one would correspond to the unoccupied subgap states formed by defects as illustrated in Fig. 10.

Finally, we examined the electronic structure of LaZnOP relative to those of related semiconductors, LaCuOS and ZnO. Figure 11 shows a band alignment diagram of these compounds built by UPS measurements, which is consistent with the band structures in Fig. 8 (note that their energies were aligned using O 2*s* levels). It is clear that ZnO has the deepest VBM level and that the VBM level rises as the constituent orbitals of the VBM change from O 2*p* (ZnO) to S 3*p* (LaCuOS) and to P 3*p* (LaZnOP). These results can be understood by the ionization energy of the corresponding

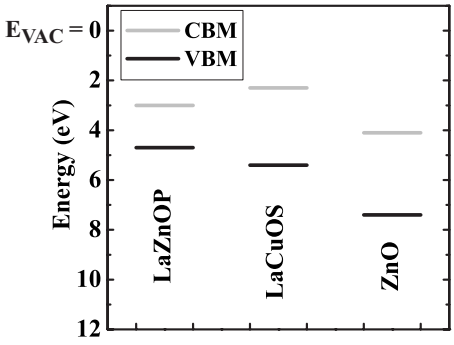

FIG. 11. Band alignment of LaZnOP, LaCuOS, and ZnO built by the UPS measurements.

anions, which increases in the order of O^{2-}, S^{2-}, and P^{3-}. Consequently, the VBM level of the oxypnictide is nearly 3 eV above that of the simple oxide, ZnO. In contrast, because the conduction bands are formed mainly by Zn 4*s* both for ZnO and LaZnOP, the energy difference of the CBM levels is smaller (~1 eV) than that of the VBM levels. (The small difference of 1 eV is due to the difference in the dispersion of the conduction band: i.e., the width of the conduction band is >3 eV for ZnO, but that is ~1.4 eV for LaZnOP as seen in Fig. 8.) Thus, the band gap of LaZnOP is smaller than that of ZnO. A similar interpretation is possible for LaCuOS. The VBM level of LaCuOS is ~1 eV lower than that of LaZnOP, but the CBM level of LaCuOS is ~0.5 eV higher than LaZnOP because the CBM of LaCuOS mainly consists of Cu 4*s* orbitals, and the conduction band has a smaller dispersion and a smaller width as seen in Fig. 8, which results in the larger band gap of LaCuOS.

IV. CONCLUSION

The electrical and optical properties of LaZnOP were examined in detail. A room-temperature electrical conductivity as high as 5.2 S/cm was obtained for Cu-doped LaZnOP. Seebeck coefficients showed negative values for the undoped LaZnOP but positive values for the Cu-doped LaZnOP, suggesting successful bipolar doping of LaZnOP. However, the absolute values of Seebeck coefficients were too small for a crystalline band semiconductor, and some samples exhibited sign inversion with varying temperature. Ultraviolet photoemission spectroscopy measurements indicated Fermi level pinning at an energy close to the conduction band minimum. The optical absorption spectrum showed two optical absorption edge structures at 1.3 and 1.7 eV. Combining these experimental results with *ab initio* calculations, we assigned the lower energy absorption edge to a defect band, which causes Fermi level pinning, and the higher energy edge to the intrinsic conduction band minimum. These findings demonstrate the importance of using multiple methods to determine carrier polarity because conventional methods such as a Hall measurement and a thermopower measurement do not always give accurate results, especially for heavily doped materials.

*Also at Frontier Research Center, Tokyo Institute of Technology, Japan.
†Also at ERATO-SORST, JST, Japan.
‡Corresponding author; also at Materials and Structures Laboratory, Tokyo Institute of Technology, Japan. hosono@msl.titech.ac.jp

[1] S. Nakamura, S. J. Pearton, and G. Fasol, *The Blue Laser Diode: The Complete Story* (Springer, New York, 2000).
[2] For a review, see H. Hiramatsu, H. Kamioka, K. Ueda, H. Ohta, T. Kamiya, M. Hirano, and H. Hosono, Phys. Status Solidi A **203**, 2800 (2006).
[3] I. Akasaki and H. Amano, Jpn. J. Appl. Phys., Part 1 **36**, 5393 (1997).
[4] Y. Nakano and T. Jimbo, J. Appl. Phys. **92**, 5590 (2002).
[5] J. Qiu, J. M. DePuydt, H. Cheng, and M. A. Haase, Appl. Phys. Lett. **59**, 2992 (1991).
[6] A. Tsukazaki, A. Ohtomo, T. Onuma, M. Ohtani, T. Makino, M. Sumiya, K. Ohtani, S. F. Chichibu, S. Fuke, Y. Segawa, H. Ohno, H. Koinuma, and M. Kawasaki, Nat. Mater. **4**, 42 (2005).
[7] H. Hiramatsu, K. Ueda, H. Ohta, M. Hirano, T. Kamiya, and H. Hosono, Appl. Phys. Lett. **82**, 1048 (2003).
[8] H. Hiramatsu, K. Ueda, H. Ohta, M. Hirano, M. Kikuchi, H. Yanagi, T. Kamiya, and H. Hosono, Appl. Phys. Lett. **91**, 012104 (2007).
[9] K. Ueda, S. Inoue, H. Hosono, N. Sarukura, and M. Hirano, Appl. Phys. Lett. **78**, 2333 (2001).
[10] K. Takase, M. Koyano, T. Shimizu, K. Makihara, Y. Takahashi, Y. Takano, and K. Sekizawa, Solid State Commun. **123**, 531 (2002).
[11] H. Hiramatsu, K. Ueda, K. Takafuji, H. Ohta, M. Hirano, T. Kamiya, and H. Hosono, J. Appl. Phys. **94**, 5805 (2003).
[12] M. Palazzi, C. R. Seances Acad. Sci., Ser. 2 **292**, 789 (1981).
[13] W. J. Zhu, Y. Z. Huang, C. Dong, and Z. X. Zhao, Mater. Res. Bull. **29**, 143 (1994).
[14] B. A. Popovkin, A. M. Kusainova, V. A. Dolgikh, and L. G. Aksel'rud, Russ. J. Inorg. Chem. **43**, 1471 (1998).
[15] D. O. Charkin, A. V. Akopyan, and V. A. Dolgikh, Russ. J. Inorg. Chem. **44**, 833 (1999).
[16] K. Takase, K. Sato, O. Shoji, Y. Takahashi, Y. Takano, K. Sekizawa, Y. Kuroiwa, and M. Goto, Appl. Phys. Lett. **90**, 161916 (2007).
[17] K. Ueda, H. Hiramatsu, H. Ohta, M. Hirano, T. Kamiya, and H. Hosono, Phys. Rev. B **69**, 155305 (2004).
[18] H. Hiramatsu, K. Ueda, H. Ohta, T. Kamiya, M. Hirano, and H. Hosono, Appl. Phys. Lett. **87**, 211107 (2005).
[19] H. Hiramatsu, K. Ueda, T. Kamiya, H. Ohta, M. Hirano, and H. Hosono, J. Mater. Chem. **14**, 2946 (2004).
[20] K. Ueda, H. Hiramatsu, M. Hirano, T. Kamiya, and H. Hosono, Thin Solid Films **496**, 8 (2006).
[21] B. I. Zimmer, W. Jeitschko, J. H. Albering, R. Glaum, and M. Reehuis, J. Alloys Compd. **229**, 238 (1995).
[22] A. T. Nientiedt, W. Jeitschko, P. G. Pollmeier, and M. Brylak, Z. Naturforsch., B: Chem. Sci. **52**, 560 (1997).
[23] A. T. Nientiedt and W. Jeitschko, Inorg. Chem. **37**, 386 (1998).
[24] P. Quebe, L. J. Terbüchte, and W. Jeitschko, J. Alloys Compd. **302**, 70 (2000).
[25] H. Lincke, T. Nilges, and R. Pöttgen, Z. Anorg. Allg. Chem. **632**, 1804 (2006).
[26] M. Orita, H. Ohta, M. Hirano, S. Narushima, and H. Hosono, Philos. Mag. B **81**, 501 (2001).
[27] Y. Takano, S. Komatsuzaki, H. Komasaki, T. Watanabe, Y. Takahashi, and K. Takase, J. Alloys Compd., doi:10.1016/j.jallcom.2007.04.203 (2007).
[28] K. Ueda, K. Takafuji, and H. Hosono (unpublished).
[29] TOPAS, Version 3, Bruker AXS, Karlsruhe, Germany, 2005.
[30] P. Kubelka and F. Munk, Z. Tech. Phys. (Leipzig) **12**, 593 (1931).
[31] G. Kresse and J. Furthmüller, Phys. Rev. B **54**, 11169 (1996).